

**Electronic Supplementary Information
for**

**Synthesis, structure, magnetic properties and thermal behaviour of
Ba-M^{II} (M^{II} = Mn, Co, Cu, Zn) allylmalonates**

Ekaterina N. Zorina-Tikhonova^{*a}, Anna K. Matyukhina^a, Aleksandr S. Chistyakov^a, Natalia V. Gogoleva^a, Veronika A. Novikova^{a,c}, Anna V. Vologzhanina^b, Alexander A. Korlyukov^b, Ekaterina V. Belova^c, Elena A. Ugolkova^a, Alyona A. Starikova^d, Denis V. Korchagin^e, Konstantin A. Babeshkin^a, Nikolay N. Efimov^a, Mikhail A. Kiskin^a and Igor L. Eremenko^{a,b}

^a*N.S. Kurnakov Institute of General and Inorganic Chemistry of the Russian Academy of Sciences, Leninsky Prospekt 31, 119991 Moscow, Russian Federation.*

E-mail: ezorinatikhonova@gmail.com

^b*A.N. Nesmeyanov Institute of Organoelement Compounds of the Russian Academy of Sciences, Vavilova str. 28, 119334 Moscow, Russian Federation*

^c*Chemistry Department, Lomonosov Moscow State University, Leninskie Gory, 1-3, 119991, Moscow, Russian Federation*

^d*Institute of Physical and Organic Chemistry, Southern Federal University, prosp. Stacki, 194/2, 344090 Rostov-on-Don, Russian Federation*

^e*Institute of Problems of Chemical Physics of the Russian Academy of Sciences, Ac. Semenov prospekt 1, 142432 Chernogolovka, Moscow region, Russian Federation*

X-ray crystal data collection

Single crystals of **1-4** were obtained from reaction mixtures. Intensities of the reflections for these crystals were collected with Bruker Apex II CCD diffractometer at 120.0(2) (for **1-3**) or 100.0(2) (for **4**) K using graphite monochromated MoK α radiation ($\lambda = 0.71073 \text{ \AA}$). The structures were solved by the SHELXT method¹ and refined by full-matrix least squares against F². Non-hydrogen atoms were refined anisotropically except for disordered fragments. Alkyl groups in **1-4** are disordered over two sites, and carbon atoms in these fragments were refined isotropically using rigid body restraints (RIGU instruction) and restraints for thermal ellipsoids (ISOR). The H(O) atoms were located on difference Fourier maps, while positions of the H(C) atoms were calculated. All hydrogen atoms were included in a refinement by the riding model with $U_{\text{iso}}(\text{H}) = 1.5U_{\text{eq}}(\text{O})$ and $1.2U_{\text{eq}}(\text{C})$ for. All calculations were made using the SHELXL2014¹ and OLEX2² program packages. Crystallographic parameters and refinement details for all complexes are listed in Table S1. CCDC 2167691-2167694 contain the supplementary crystallographic data for this paper. These data can be obtained free of charge via <http://www.ccdc.cam.ac.uk/structures/>.

Table S1 Crystallographic parameters and structure refinement statistics for complexes **1–4**

Compound	1	2	3	4
Empirical formula	C ₁₂ H ₁₈ BaMnO ₁₁	C ₁₂ H ₁₈ BaCoO ₁₁	C ₁₂ H ₁₈ BaCuO ₁₁	C ₁₂ H ₁₈ BaO ₁₁ Zn
Formula weight	530.54	534.53	539.14	540.97
Crystal system	Trigonal	Trigonal	Monoclinic	Trigonal
Space group	R-3	R-3	P2 ₁ /c	R-3
a [Å]	24.7609(4)	24.7322(11)	12.313(2)	24.7462(7)
b [Å]	24.7609(4)	24.7322(11)	24.650(4)	24.7462(7)
c [Å]	14.5331(3)	14.3209(7)	17.294(3)	14.3059(9)
β [°]	90	90	99.921(4)	90
Volume [Å ³]	7716.5(3)	7586.2(8)	5170.5(2)	7586.9(6)
Z	18	18	12	18
ρ _{calc} [g/cm ³]	2.055	2.106	2.078	2.131
μ [mm ⁻¹]	3.074	3.361	3.559	3.800
F(000)	4662	4698	3156	4752
Crystal size/mm ³	0.30 × 0.28 × 0.28	0.39 × 0.28 × 0193	0.40 × 0.30 × 0.19	0.41 × 0.29 × 0.18
Reflections collected	31886	28904	66003	12694
Independent reflections	5248 [R _{int} = 0.0267]	5191 [R _{int} = 0.0481]	15863 [R _{int} = 0.1027]	6090 [R _{int} = 0.0628]
Data/restraints/parameters	5248/0/218	5191/6/230	15863/20/671	6090/6/223
Goodness-of-fit on F ²	1.040	1.117	1.084	1.013

Final R indexes [I>=2σ (I)]	R1 = 0.0376, 0.0913	wR2 = R ₁ = 0.0369, 0.0694	wR ₂ = R ₁ = 0.0769, wR ₂ = 0.1871	R ₁ = 0.0464, wR ₂ = 0.0903
Final R indexes [all data]	R1 = 0.0392, 0.0921	wR2 = R ₁ = 0.0450, 0.0719	wR ₂ = R ₁ = 0.1871, wR ₂ = 0.2063	R ₁ = 0.0609, wR ₂ = 0.0955
Largest diff. peak/hole/eÅ ⁻³	2.06/-2.12	1.54/-1.35	5.86/-4.01	2.28/-1.98

PXRD

The PXRD data in the form of powder patterns were collected on a Bruker D8 Advance diffractometer (Bruker, Billerica, MA, USA) with a LynxEye detector in Bragg-Brentano geometry, with the sample thinly dispersed on a zero-background Si sample holder, $\lambda(\text{CuK}\alpha) = 1.54060 \text{ \AA}$, θ/θ scan with variable slits (irradiated length 20 mm), 2θ from 5° to 41° , step size 0.02° .

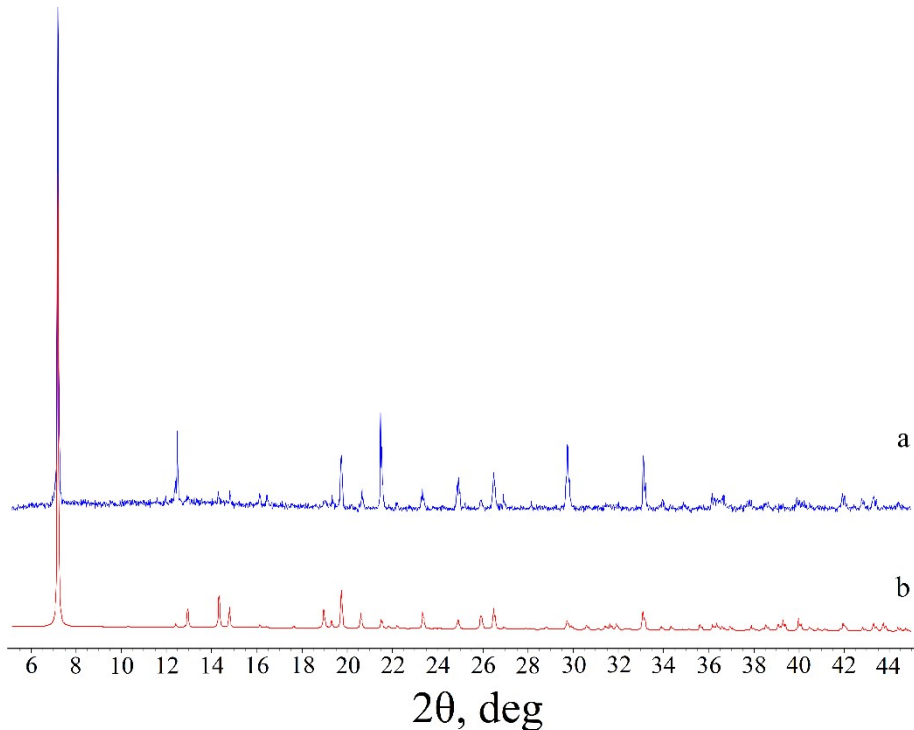


Figure S1. XRD powder patterns for compound 1: experimental (a), calculated (b)

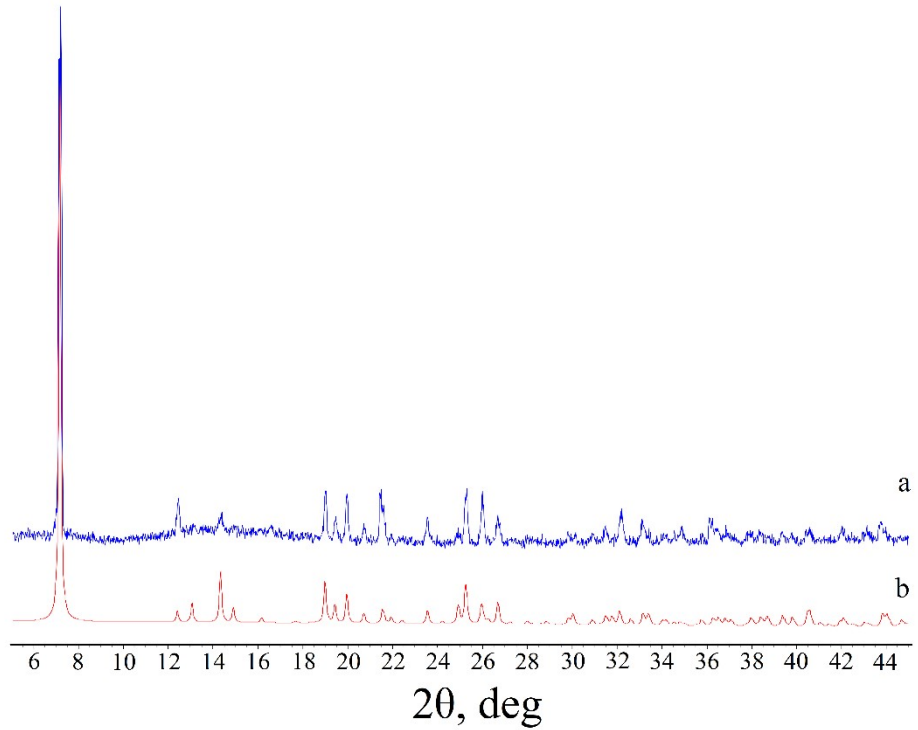


Figure S2. XRD powder patterns for compound 2: experimental (*a*), calculated (*b*)

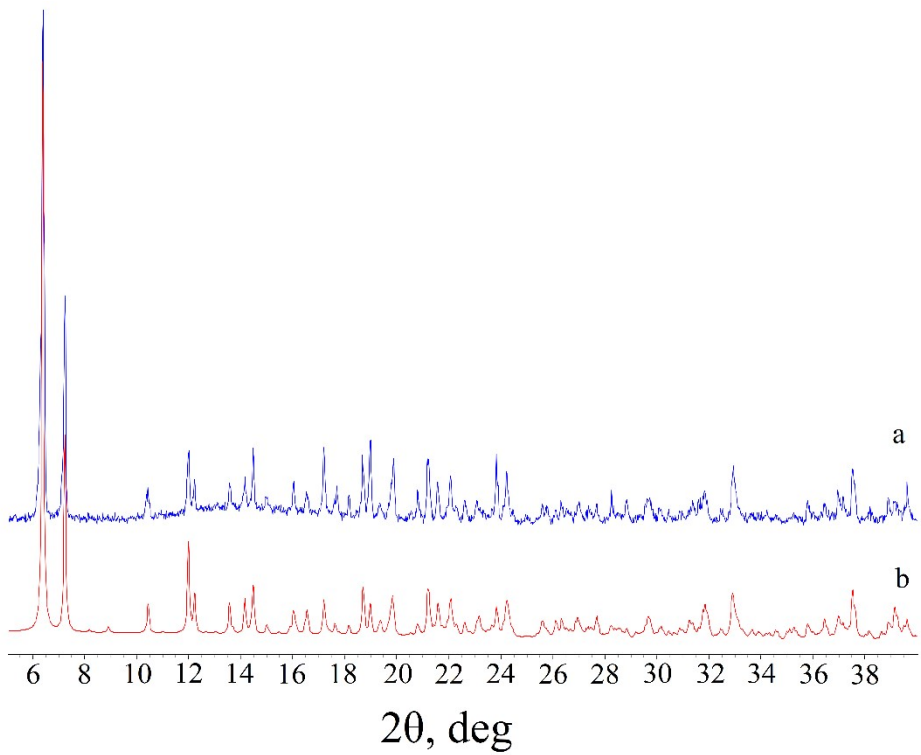


Figure S3. XRD powder patterns for compound 3: experimental (*a*), calculated (*b*)

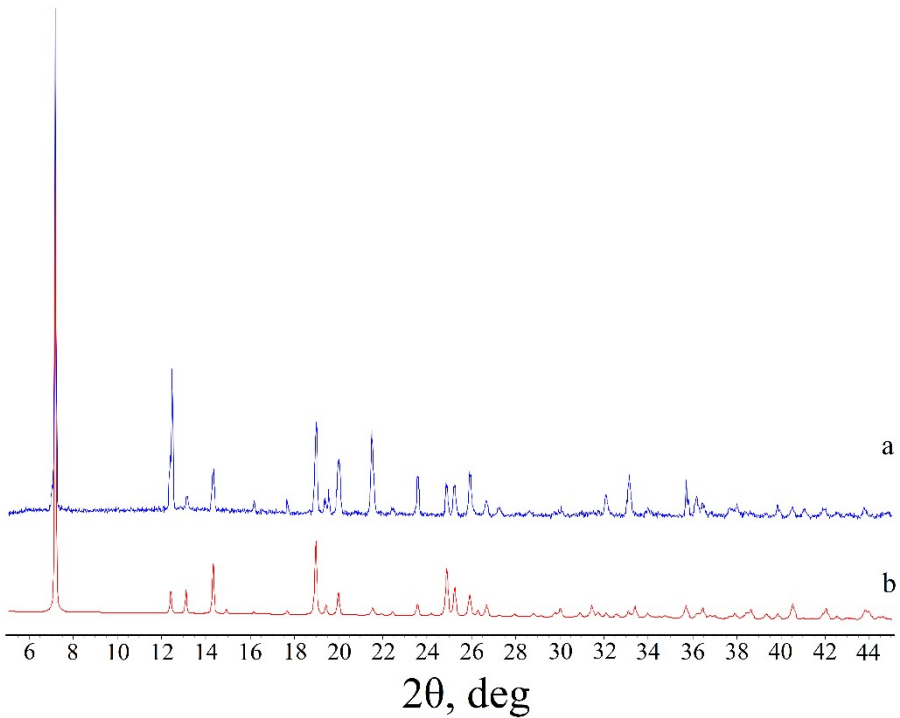


Figure S4. XRD powder patterns for compound 4: experimental (*a*), calculated (*b*)

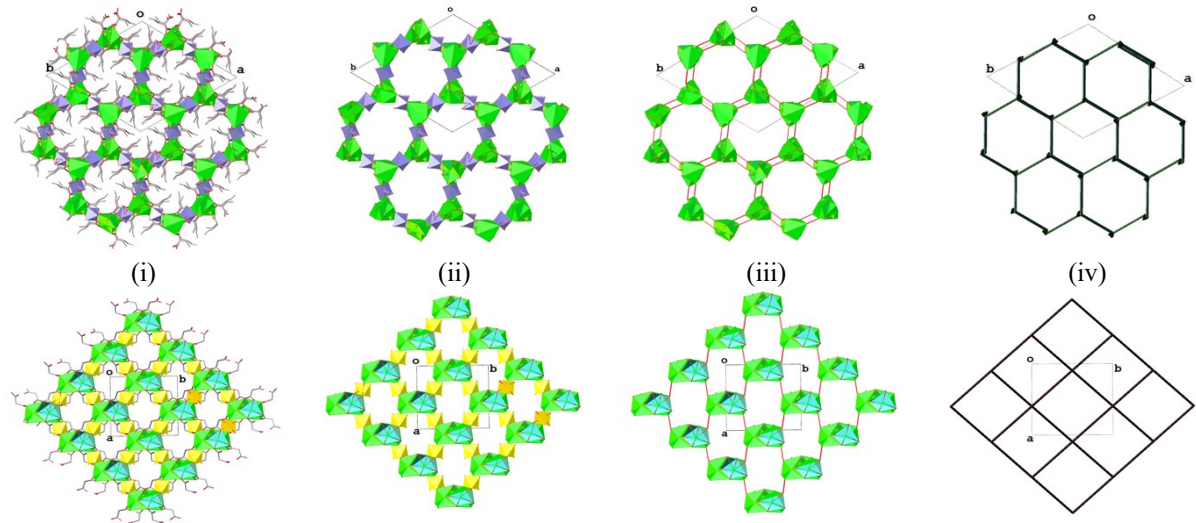


Figure S5. Simplification procedure to estimate topology of underlying nets in rod packings. (i) Fragment of crystal packing for (top) **1** and (bottom) $[\text{BaNi}(\text{mal})_2(\text{H}_2\text{O})_3]_n$. (ii) Carbon and hydrogen atoms were removed to obtain BaO_n -containing rods (green) connected by MnO_6 (violet) or NiO_6 (yellow) polyhedra. (iii) Transition metals were removed keeping connectivity of rods. (iv) Connectivity of rod central lines was used to reveal topology of their underlying nets.

EPR spectroscopy

The X-band EPR spectra for **1** and **3** were recorded on a Bruker Elexsys E680-X spectrometer at T = 294 K.

The spectra of compounds **1** and **3** recorded at room temperature are described by a spin Hamiltonian (SH) with a fine structure with full spin S = 5/2 for manganese in **1** and S = 1 for copper in **3**:

$$\hat{H} = \beta(g_x S_x H_x + g_y S_y H_y + g_z S_z H_z) + D(S_z^2 - S(S+1)/3) + E(S_x^2 - S_y^2)$$

where S_x , S_y , S_z are the projections of full spin on axes x, y and z, respectively; D and E are the components of the fine interaction tensor; g_x , g_y and g_z are the components of the g-tensor; H is the applied magnetic field.

In this work, a computer simulation of the EPR spectrum of compound **1** was performed using the Belford method (eigenfield method)³. The computer simulation of the EPR spectrum of compound **3** was performed by the method described in Ref. 4. The sum of the Lorentz and Gauss functions was used as the line shape function.⁵ g-factors, line widths and shapes and fine interaction tensor components were varied in the course of minimization. The best \mathbf{D} and \mathbf{E} parameters and g-tensor components are shown in the Table of EPR data. The values of g-factors obtained are close to the calculated ones found from the magnetic data for compounds **1** and **3**, which confirms the absence of strong exchange interactions between paramagnetic centers.

Table S2. The best-fit values of SH for complex **1** and **3**

	1	3
g_x	1.995	2.066
g_y	1.995	2.092
g_z	1.995	2.229
g_{iso}	1.995	2.129
D , cm ⁻¹	$6.10 \cdot 10^{-2}$	$5.25 \cdot 10^{-3}$
E , cm ⁻¹	$1.19 \cdot 10^{-2}$	$2.99 \cdot 10^{-4}$

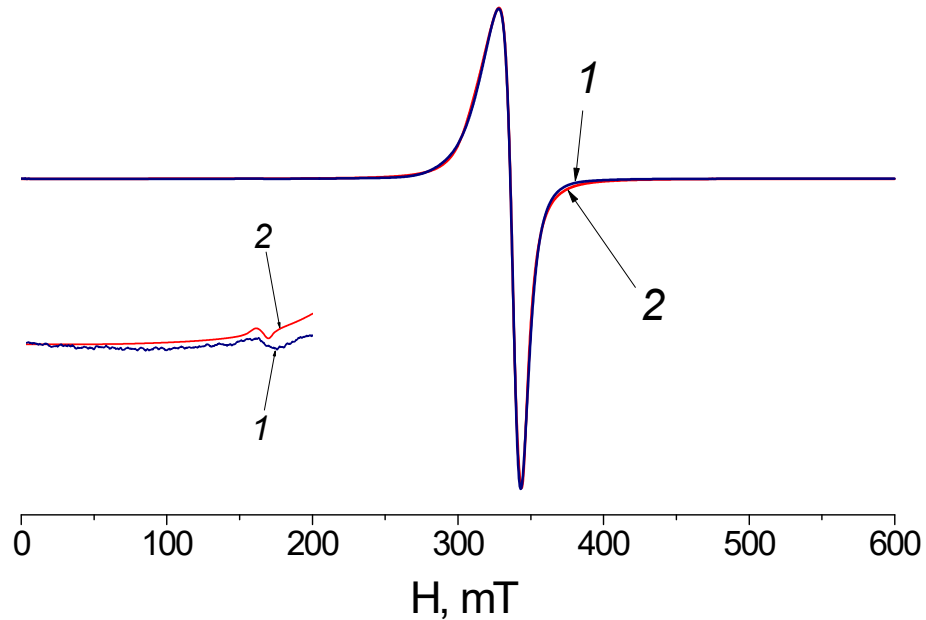


Figure S6. EPR spectrum of compound 1, experiment (1), simulation with SH parameters (2)

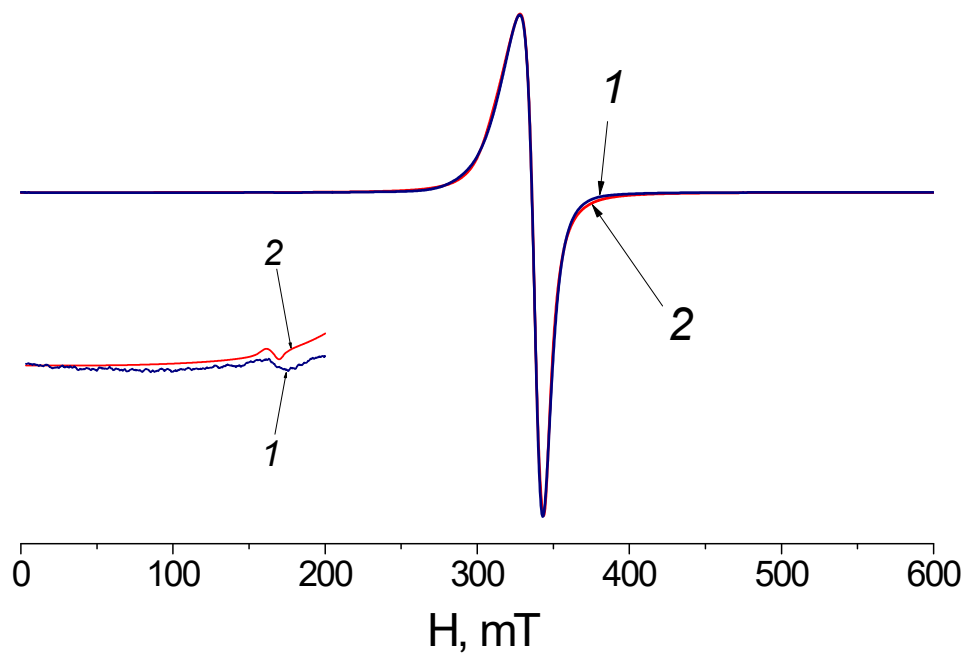


Figure S7. EPR spectrum of compound 3, experiment (1), simulation with SH parameters (2)

Magnetic properties

The magnetic behavior was studied using the Quantum Design PPMS-9 physical property measuring system with the option of measuring dynamic (ac) and static (dc) magnetic susceptibility. This equipment allows research to be carried out in the temperature range of 2–300 K with magnetic fields up to 9 T. During ac susceptibility measurements, an alternating magnetic field amplitude was $H_{ac} = 1\text{--}5$ Oe in the frequency range 10 000–10 Hz. The measurements were carried out on polycrystalline samples

moistened with mineral oil to prevent the orientation of the crystals in dc magnetic field. The prepared samples were sealed in plastic bags. The magnetic susceptibility χ was determined taking into account the diamagnetic contribution of the substance, using the Pascal scheme, the contribution of the bag and that of mineral oil.

AC-magnetic properties

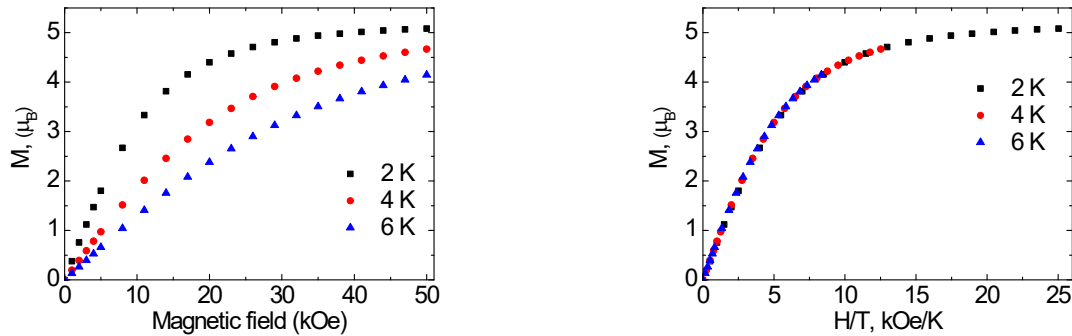


Figure S8. The $M(H)$ and $M(H/T)$ dependences at different temperatures for complex **1**

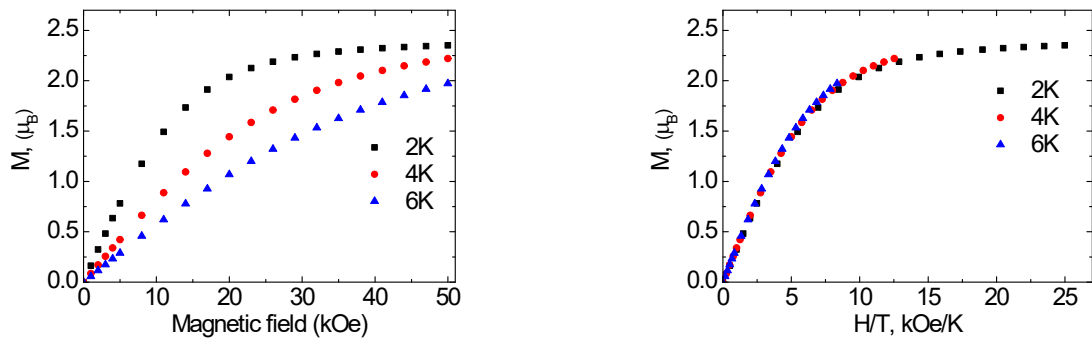


Figure S9. The $M(H)$ and $M(H/T)$ dependences at different temperatures for complex **2**

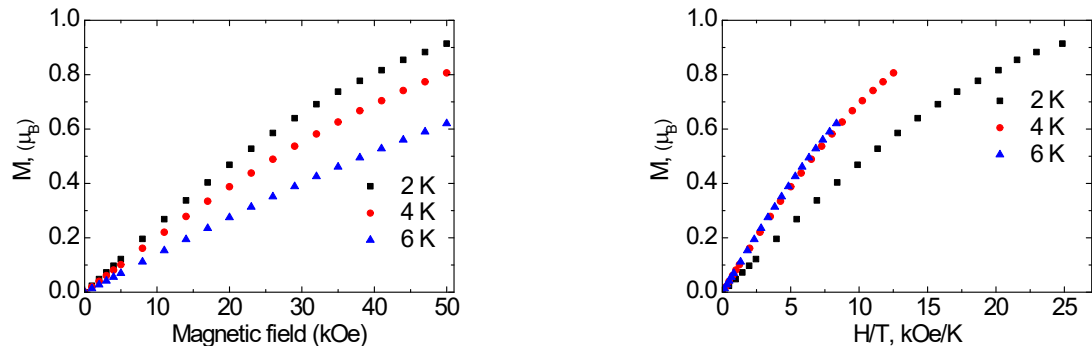


Figure S10. The $M(H)$ and $M(H/T)$ dependences at different temperatures for complex **3**.

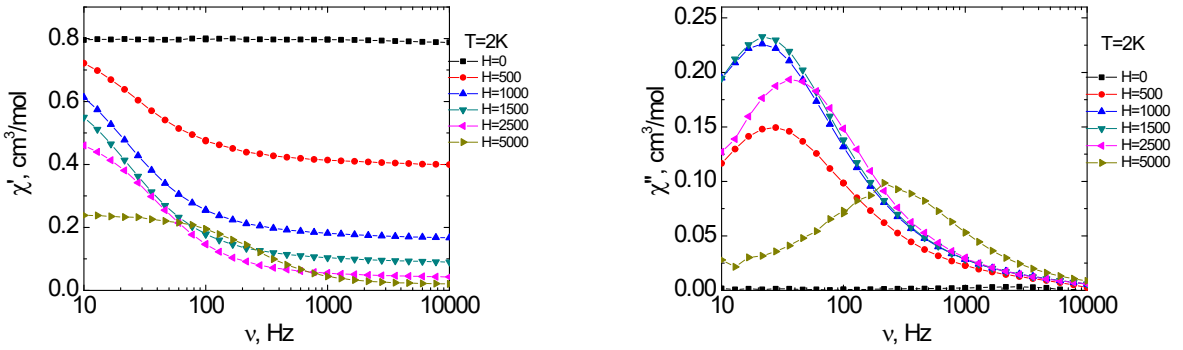
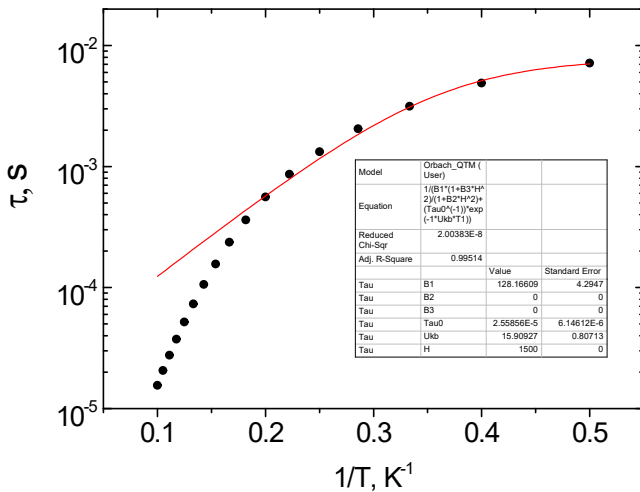


Figure S11. Frequency dependencies of real, χ' (left) and imaginary, χ'' (right) components of dynamic magnetic susceptibility for complex **2** at $T = 2$ K under various dc magnetic fields. Solid lines are visual guides.

Table S3. Fitting of the τ vs. T dependences for **2**

Dependence of the relaxation time τ on the reciprocal temperature for complex 2 ($H = 1.5$ kOe, $T = 2\text{--}10$ K)	Fit function, temperature range, and the best-fit parameters with uncertainties.																																				
<table border="1"> <caption>Fit parameters for Exp2PMod1 (Blue Line)</caption> <thead> <tr> <th>Model</th><th>Equation</th><th>y = a*exp(b*x)</th></tr> </thead> <tbody> <tr> <td>Reduced Chi-Sqr</td><td></td><td>4.3513E-14</td></tr> <tr> <td>Adj. R-Square</td><td></td><td>0.99881</td></tr> <tr> <td>Tau</td><td>a</td><td>9.317E-8</td></tr> <tr> <td></td><td>b</td><td>51.23755</td></tr> <tr> <td></td><td></td><td>1.29746</td></tr> </tbody> </table> <table border="1"> <caption>Fit parameters for Exp2PMod1 (Red Line)</caption> <thead> <tr> <th>Model</th><th>Equation</th><th>y = a*exp(b*x)</th></tr> </thead> <tbody> <tr> <td>Reduced Chi-Sqr</td><td></td><td>3.08549E-7</td></tr> <tr> <td>Adj. R-Square</td><td></td><td>0.92512</td></tr> <tr> <td>Tau</td><td>a</td><td>1.97736E-4</td></tr> <tr> <td></td><td>b</td><td>7.32937</td></tr> <tr> <td></td><td></td><td>0.63559</td></tr> </tbody> </table>	Model	Equation	y = a*exp(b*x)	Reduced Chi-Sqr		4.3513E-14	Adj. R-Square		0.99881	Tau	a	9.317E-8		b	51.23755			1.29746	Model	Equation	y = a*exp(b*x)	Reduced Chi-Sqr		3.08549E-7	Adj. R-Square		0.92512	Tau	a	1.97736E-4		b	7.32937			0.63559	<p>Orbach</p> $\tau = \tau_0 \cdot \exp(\Delta E/kT)$ $T = 9\text{--}10 \text{ K}$ $\Delta E/k = 51 \pm 1 \text{ K}$ $\tau_0 = 9 \cdot 10^{-8} \pm 1 \cdot 10^{-8} \text{ s}$ $R^2 = 0.99881 \text{ (blue line)}$ $T = 2\text{--}10 \text{ K}$ $\Delta E/k = 7.3 \pm 0.6 \text{ K}$ $\tau_0 = 2.0 \cdot 10^{-4} \pm 6 \cdot 10^{-5} \text{ s}$ $R^2 = 0.92512 \text{ (red line)}$ <p><i>Unsatisfactory fit</i></p>
Model	Equation	y = a*exp(b*x)																																			
Reduced Chi-Sqr		4.3513E-14																																			
Adj. R-Square		0.99881																																			
Tau	a	9.317E-8																																			
	b	51.23755																																			
		1.29746																																			
Model	Equation	y = a*exp(b*x)																																			
Reduced Chi-Sqr		3.08549E-7																																			
Adj. R-Square		0.92512																																			
Tau	a	1.97736E-4																																			
	b	7.32937																																			
		0.63559																																			



Orbach + QTM

$$\tau^I = \tau_0^{-1} \cdot \exp(-\Delta E/kT) + B$$

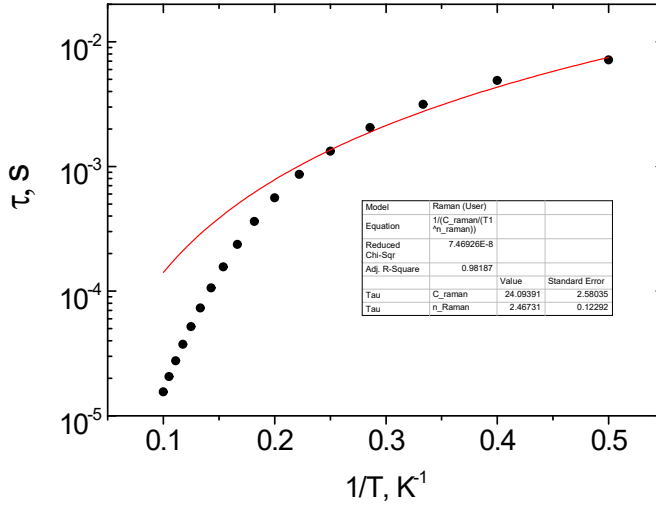
$$T = 2-10 \text{ K}$$

$$\Delta E/k = 15.9 \pm 0.8 \text{ K}$$

$$\tau_0 = 2.6 \cdot 10^{-5} \pm 6 \cdot 10^{-6} \text{ s}$$

$$B = 128 \pm 4 \text{ s}^{-1}$$

$$R^2 = 0.99514$$



Raman

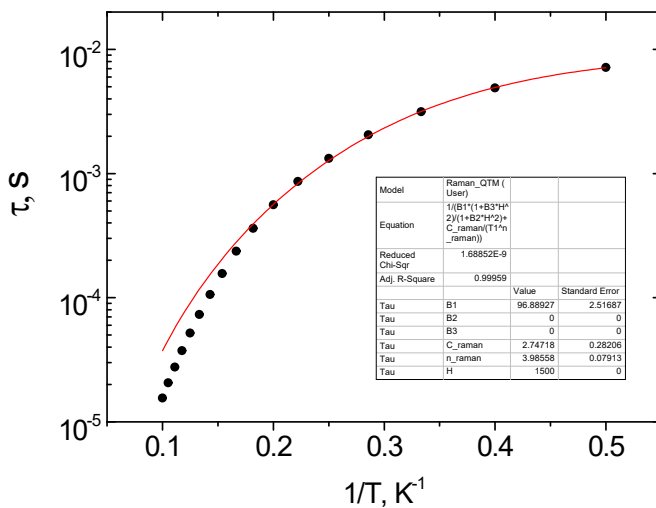
$$\tau^{-1} = C_{\text{Raman}} T^{n_{\text{Raman}}}$$

$$T = 2-10 \text{ K}$$

$$C_{\text{Raman}} = 24 \pm 3 \text{ s}^{-1} \text{K}^{-n_{\text{Raman}}}$$

$$n_{\text{Raman}} = 2.5 \pm 0.1$$

$$R^2 = 0.98187$$



Raman + QTM

$$\tau^{-1} = C_{\text{Raman}} T^{n_{\text{Raman}}} + B$$

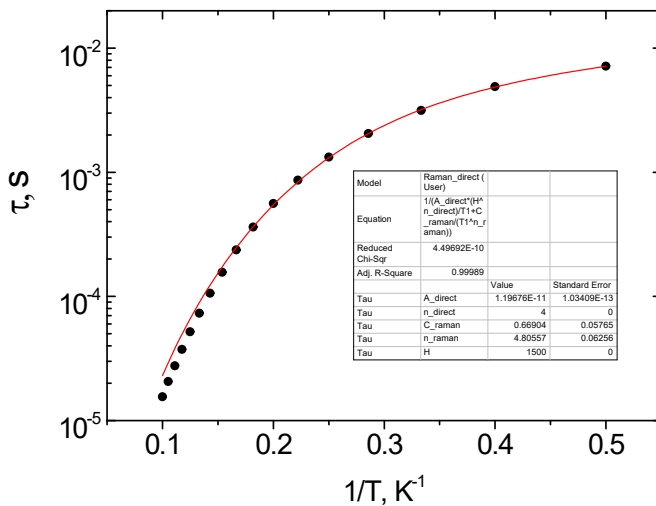
$$T = 2-10 \text{ K}$$

$$C_{\text{Raman}} = 2.7 \pm 0.3 \text{ s}^{-1} \text{K}^{-n_{\text{Raman}}}$$

$$n_{\text{Raman}} = 3.99 \pm 0.08$$

$$B = 97 \pm 3 \text{ s}^{-1}$$

$$R^2 = 0.99959$$



Raman + Direct

$$\tau^{-1} = C_{\text{Raman}} T^{\text{nRaman}} + A_{\text{direct}} TH^4$$

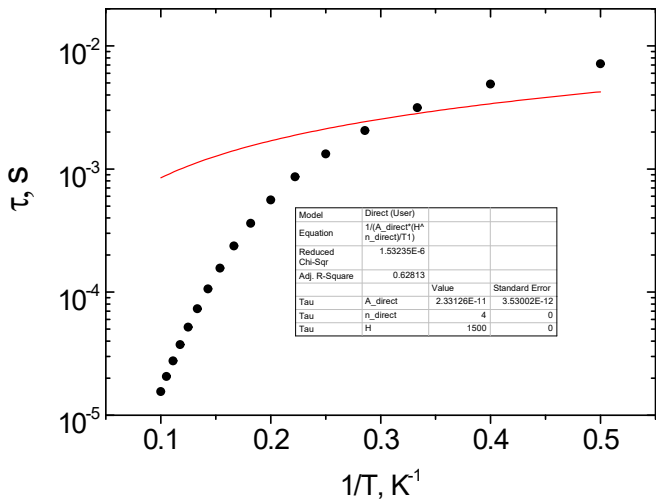
$T = 2\text{-}10 \text{ K}$

$$C_{\text{Raman}} = 0.67 \pm 0.06 \text{ s}^{-1} \text{K}^{-\text{nRaman}}$$

$$n_{\text{Raman}} = 4.81 \pm 0.06$$

$$A_{\text{direct}} = 1.20 \cdot 10^{-11} \pm 1 \cdot 10^{-13} \text{ K}^{-1} \text{Oe}^{-4} \text{s}^{-1}$$

$$R^2 = 0.99989$$



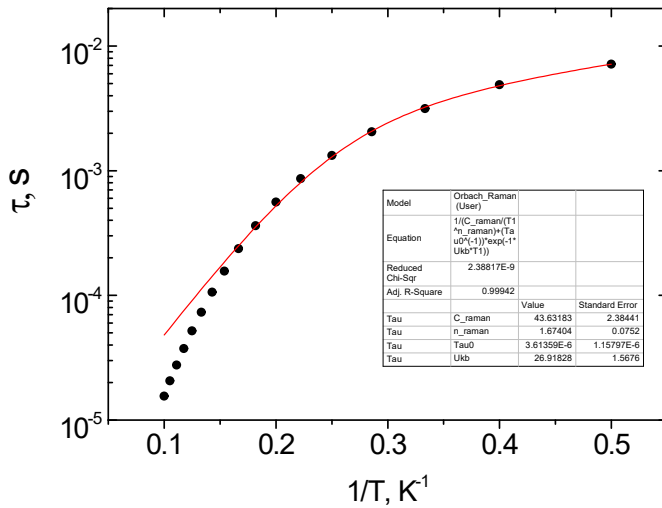
Direct

$$\tau^{-1} = A_{\text{direct}} TH^4$$

$T = 2\text{-}10 \text{ K}$

$$A_{\text{direct}} = 2.3 \cdot 10^{-11} \pm 4 \cdot 10^{-12} \text{ K}^{-1} \text{Oe}^{-4} \text{s}^{-1}$$

$$R^2 = 0.62813$$



Orbach + Raman

$$\tau^{-1} = \tau_0^{-1} \cdot \exp(-\Delta E/kT) + C_{\text{Raman}} T^{\text{nRaman}}$$

$T = 2\text{-}10 \text{ K}$

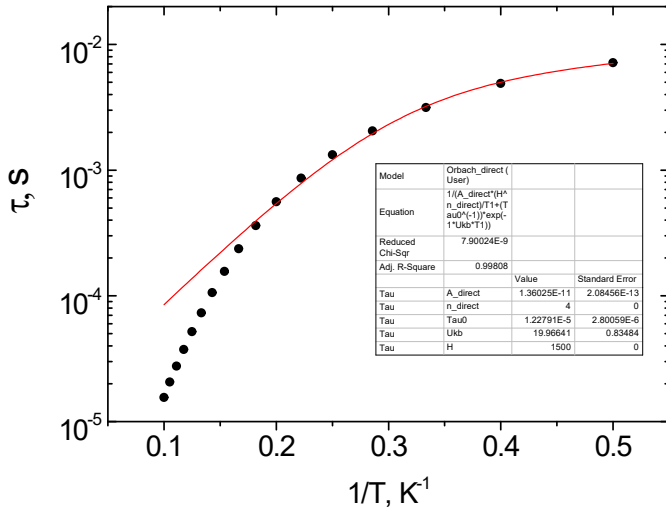
$$\Delta E/k = 27 \pm 2 \text{ K}$$

$$\tau_0 = 4 \cdot 10^{-6} \pm 1 \cdot 10^{-6} \text{ s}$$

$$C_{\text{Raman}} = 44 \pm 2 \text{ s}^{-1} \text{K}^{-\text{nRaman}}$$

$$n_{\text{Raman}} = 1.67 \pm 0.08$$

$$R^2 = 0.99942$$



Orbach + Direct

$$\tau^{-1} = \tau_0^{-1} \cdot \exp(-\Delta E/kT) + A_{\text{direct}} TH^4$$

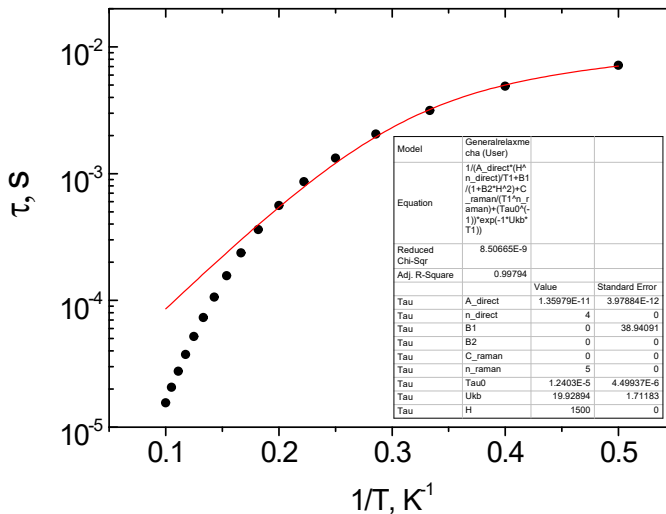
$T = 2\text{-}10 \text{ K}$

$$\Delta E/k = 20.0 \pm 0.8 \text{ K}$$

$$\tau_0 = 1.2 \cdot 10^{-5} \pm 3 \cdot 10^{-6} \text{ s}$$

$$A_{\text{direct}} = 1.36 \cdot 10^{-11} \pm 2 \cdot 10^{-13} \text{ K}^{-1} \text{Oe}^{-4} \text{s}^{-1}$$

$$R^2 = 0.99808$$



Orbach + Direct + QTM

$$\tau^{-1} = \tau_0^{-1} \cdot \exp(-\Delta E/kT) + B + A_{\text{direct}} TH^4$$

$T = 2\text{-}10 \text{ K}$

$$\Delta E/k = 20 \pm 2 \text{ K}$$

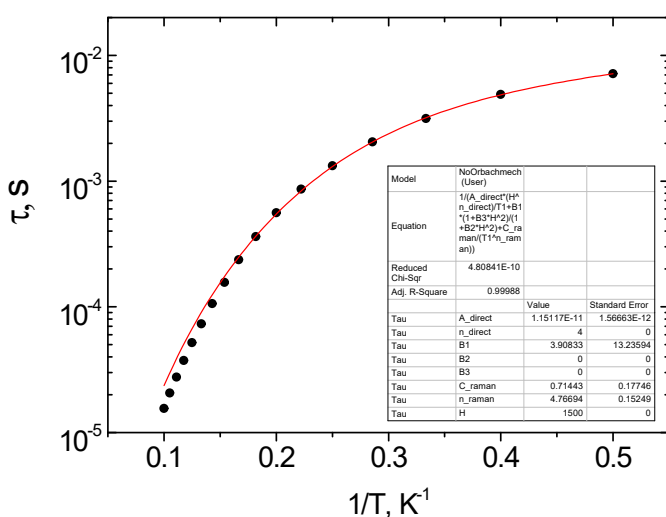
$$\tau_0 = 1.2 \cdot 10^{-5} \pm 4 \cdot 10^{-6} \text{ s}$$

$$A_{\text{direct}} = 1.4 \cdot 10^{-11} \pm 4 \cdot 10^{-12} \text{ K}^{-1} \text{Oe}^{-4} \text{s}^{-1}$$

$$B = 0 \pm 39$$

$$R^2 = 0.99794$$

Over-parametrization



Raman + Direct + QTM

$$\tau^{-1} = C_{\text{Raman}} T^n \text{Raman} + B + A_{\text{direct}} TH^4$$

$T = 2\text{-}10 \text{ K}$

$$C_{\text{Raman}} = 0.7 \pm 0.2 \text{ s}^{-1} \text{K}^{-n_{\text{Raman}}}$$

$$n_{\text{Raman}} = 4.8 \pm 0.2$$

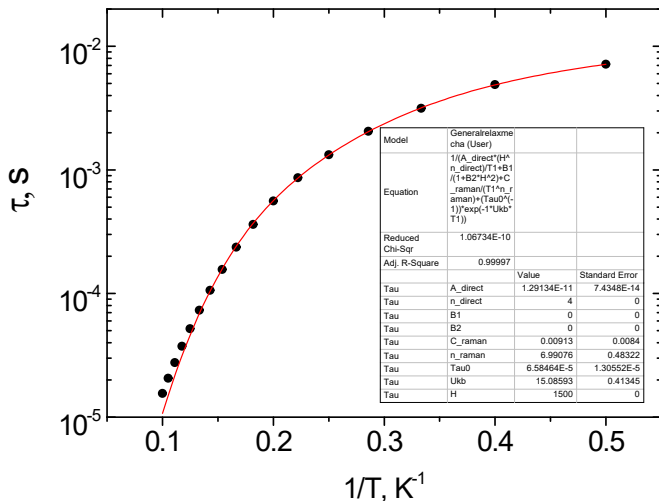
$$A_{\text{direct}} = 1.2 \cdot 10^{-11} \pm 2 \cdot 10^{-12} \text{ K}^{-1} \text{Oe}^{-4} \text{s}^{-1}$$

$$B = 4 \pm 13$$

$$R^2 = 0.99988$$

Over-parametrization

Orbach + Raman + Direct



$$\tau^{-1} = \tau_0^{-1} \cdot \exp(-\Delta E/kT) + C_{\text{Raman}} T^{n_{\text{Raman}}} + A_{\text{direct}} T H^4$$

$T = 2\text{-}10 \text{ K}$

$$\Delta E/k = 15.1 \pm 0.4 \text{ K}$$

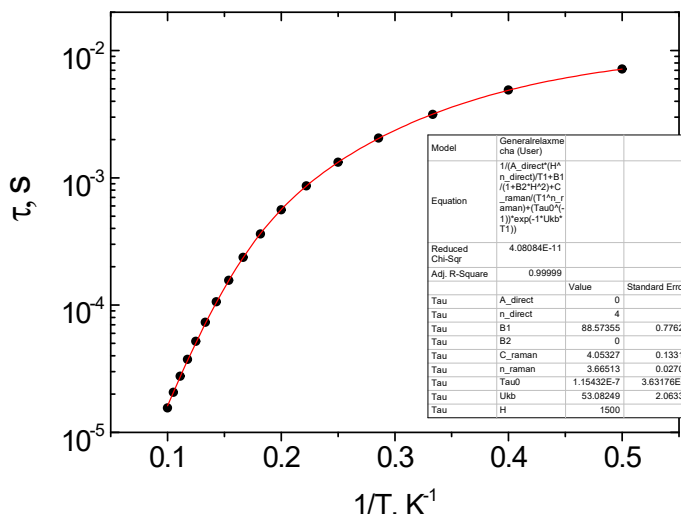
$$\tau_0 = 7 \cdot 10^{-5} \pm 1 \cdot 10^{-5} \text{ s}$$

$$C_{\text{Raman}} = 9 \cdot 10^{-3} \pm 8 \cdot 10^{-3} \text{ s}^{-1} \text{K}^{-n_{\text{Raman}}}$$

$$n_{\text{Raman}} = 7.0 \pm 0.5$$

$$A_{\text{direct}} = 1.291 \cdot 10^{-11} \pm 7 \cdot 10^{-14} \text{ K}^{-1} \text{Oe}^{-4} \text{s}^{-1}$$

$$R^2 = 0.99997$$



Orbach + Raman + QTM

$$\tau^{-1} = \tau_0^{-1} \cdot \exp(-\Delta E/kT) + C_{\text{Raman}} T^{n_{\text{Raman}}} + B$$

$T = 2\text{-}10 \text{ K}$

$$\Delta E/k = 53 \pm 2 \text{ K}$$

$$\tau_0 = 1.2 \cdot 10^{-7} \pm 4 \cdot 10^{-8} \text{ s}$$

$$C_{\text{Raman}} = 4.1 \pm 0.1 \text{ s}^{-1} \text{K}^{-n_{\text{Raman}}}$$

$$n_{\text{Raman}} = 3.67 \pm 0.03$$

$$B = 88.6 \pm 0.8$$

$$R^2 = 0.99999$$

Best fit

TGA/DSC

Samples were placed in Al_2O_3 crucibles without lid. Mass changes of the samples were determined on TG 209 F1 Iris (NETZSCH) thermobalance in a temperature range 35-900°C. The measurements were performed at scanning rate 10 K/min in argon atmosphere (gas flow 30 ml/min, protective gas flow 20 ml/min). Evolved gas was analyzed via quadrupole mass spectrometer QMS 403 Aëlos connected with the thermobalance (transfer line heated up to 290°C).

Heat flow was registered on a differential scanning calorimeter DSC 204 F1 Phoenix (NETZSCH) in a temperature range 20-520°C with the same heating rate 10 K/min in argon atmosphere (gas flow 40 ml/min, protective gas flow 70 ml/min). The calorimeter was previously calibrated both for sensitivity and temperature in the measurement range by enthalpy and temperature of phase transitions of the standards with a high (99.99%) purity Hg, In, Sn, Zn, Bi, Pb, CsCl (NETSCH) at the heating rate 10

K/min.

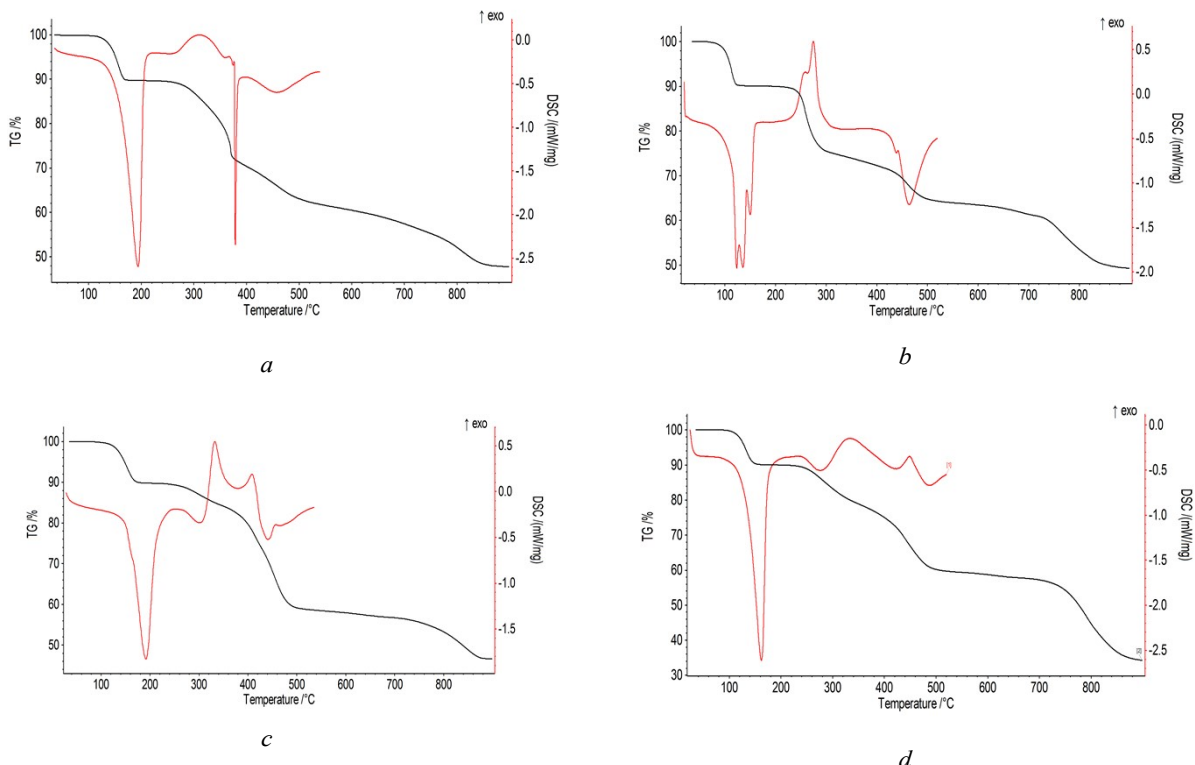


Figure S12. TG and DSC curves in Ar atmosphere at HR 10 K/min for **2** (Co) (a), **3** (Cu) (b), **1** (Mn) (c), **4** (Zn) (d)

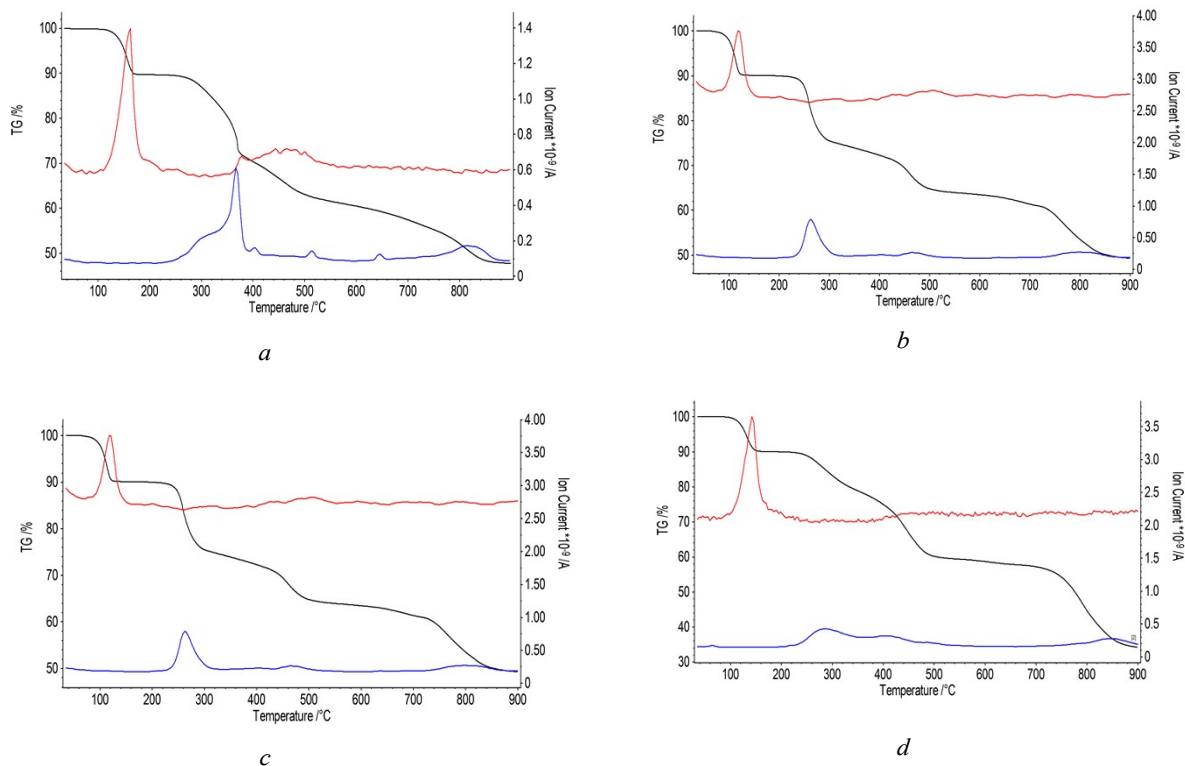
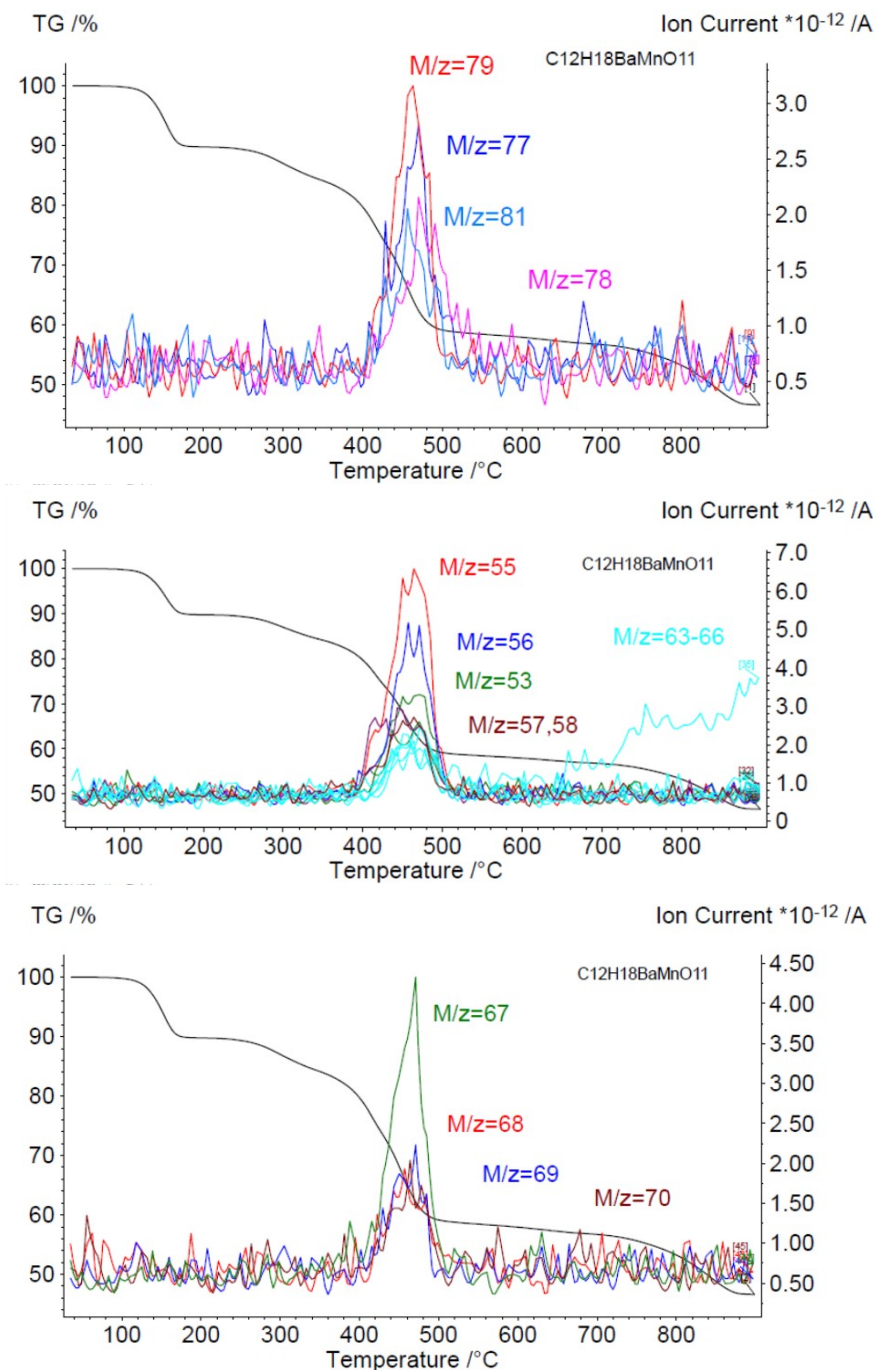


Figure S13. Mass change (black) and ion currents for $[\text{H}_2\text{O}]^+$ (red) and $[\text{CO}_2]^+$ (blue) in Ar atmosphere at HR 10 K/min for **2** (Co) (a), **3** (Cu) (b), **1** (Mn) (c), **4** (Zn) (d)



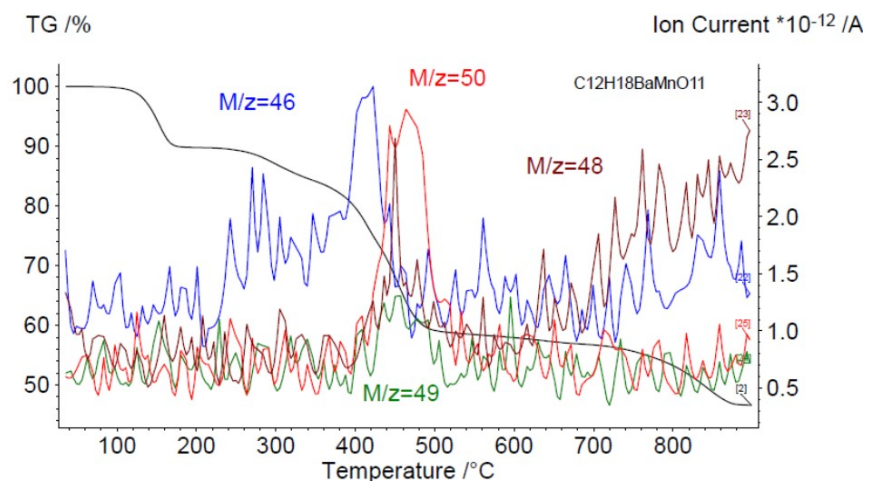


Figure S14. Mass change and ion currents in Ar atmosphere at HR 10 K/min for compound 1

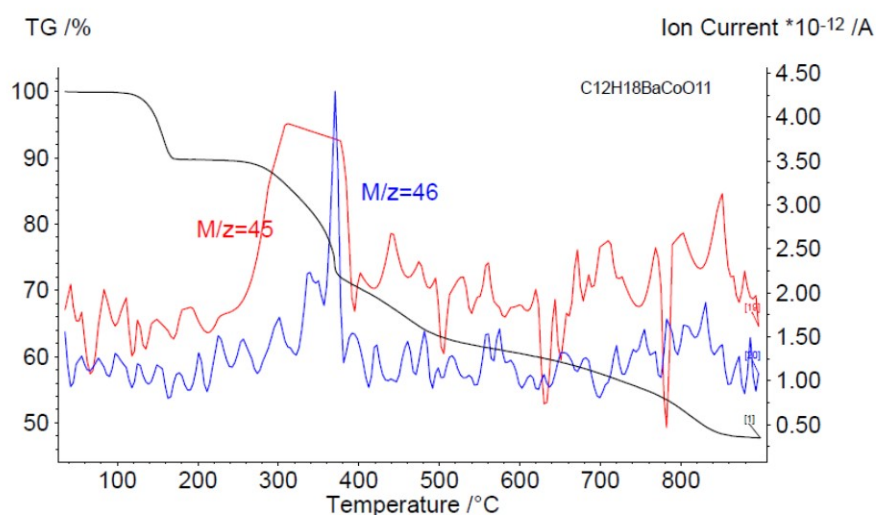


Figure S15. Mass change and ion currents in Ar atmosphere at HR 10 K/min for compound 2

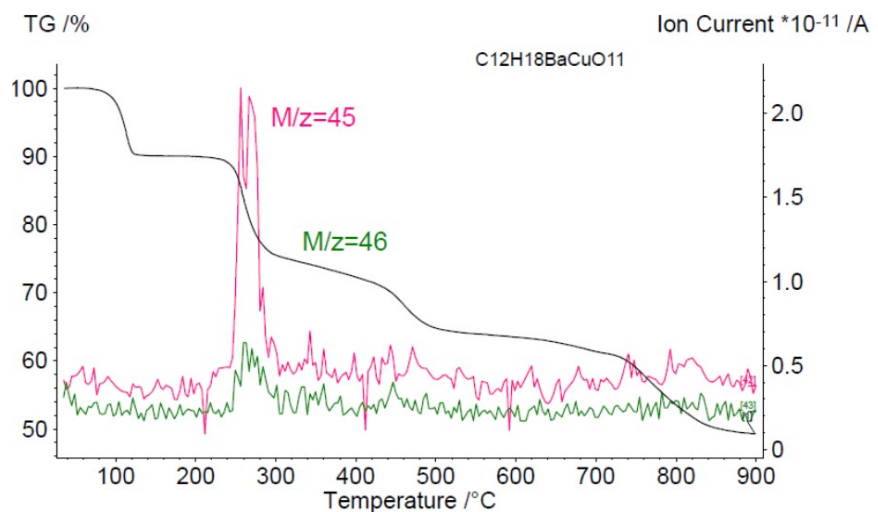


Figure S16. Mass change and ion currents in Ar atmosphere at HR 10 K/min for compound 3

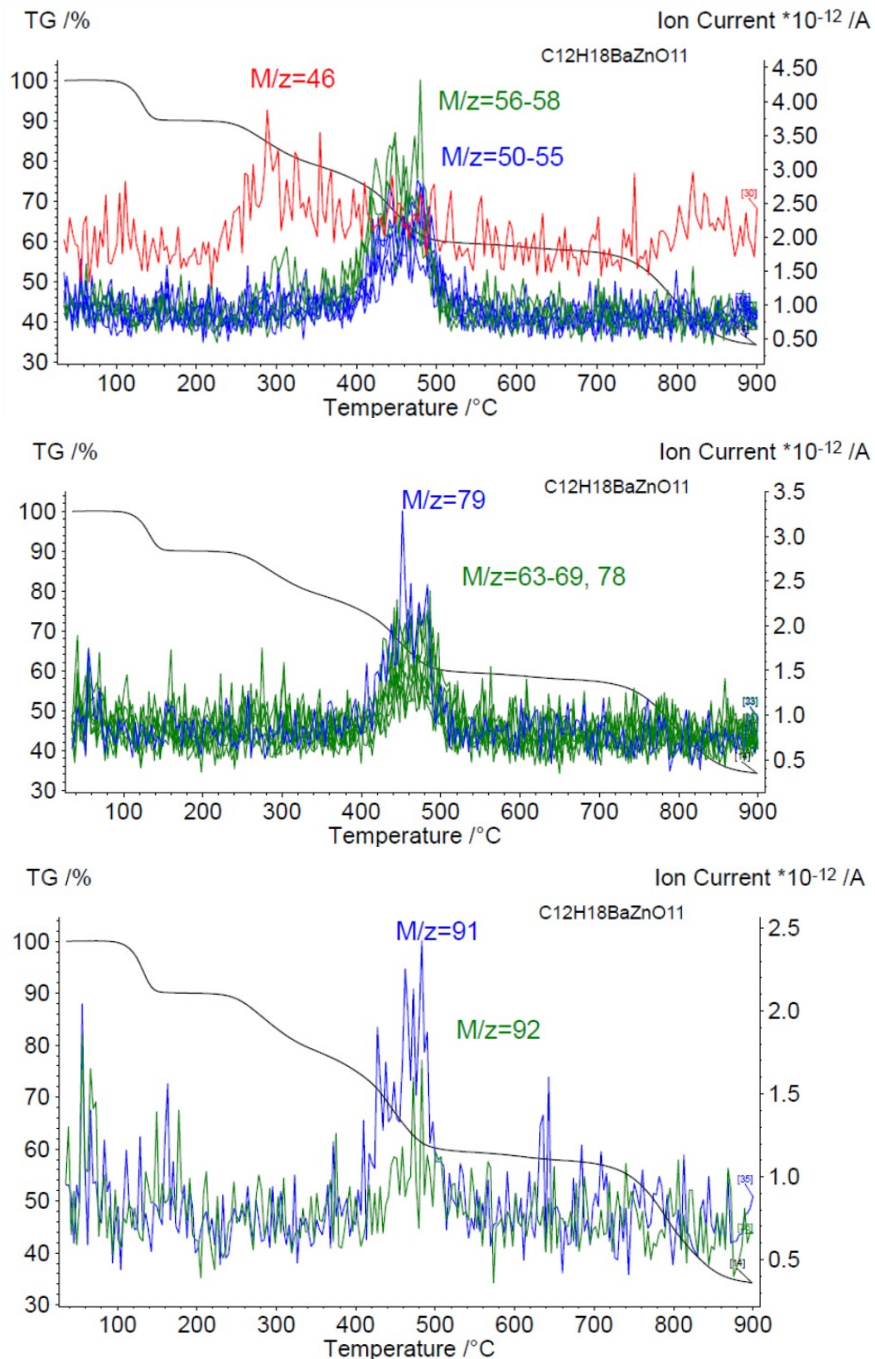


Figure S17. Mass change and ion currents in Ar atmosphere at HR 10 K/min for compound **4**

DFT calculations and Computational details

The density functional theory (DFT) calculations were performed by means of Gaussian 16 program package⁶ using UB3LYP functional⁷ reproducing well characteristics of metal coordination compounds⁸⁻¹⁰ with combination of Def2-SVP and Def2-TZVP and basis sets. Exchange interactions between paramagnetic centers were estimated applying the “broken symmetry” approach¹¹. The exchange coupling parameters J were calculated with the use of Yamaguchi equation¹².

Quantum chemical calculations of the isolated anionic Co(II) complex in **2** were performed using a post-Hartree–Fock multi-reference wavefunction (WF) approach based on state-averaged complete active space self-consistent field calculations (SA-CASSCF)¹³⁻¹⁵ followed by N-electron valence second-order perturbation theory (NEVPT2).¹⁶⁻¹⁹ Scalar relativistic effects were account for using a standard second-order Douglas–Kroll–Hess (DKH) procedure.²⁰ For calculations, a segmented all-electron

relativistically contracted version²¹ of Ahlrichs polarized triple-zeta basis set, def2-TZVP,²²⁻²⁴ was used for all atoms. To improve the calculation time, the resolution of the identity approximation with corresponding correlation fitting of the basis set²⁵ was employed. Spin-orbit effects were included using the quasi-degenerate perturbation theory (QDPT).²⁶

The CASSCF active space was constructed from 5 MOs with predominant contributions of 3d-AOs from the metal center and 7 electrons, corresponding to metal ion CAS(7, 5). Ten quartets and 40 doublet states were included in the WF expansion.

References

- 1 G. M. Sheldrick, *Acta Cryst.*, 2008, **A64**, 112.
- 2 O. V. Dolomanov, L. J. Bourhis, R. J. Gildea, J. A. K. Howard and H. Puschmann, *J. Appl. Cryst.*, 2009, **42**, 339.
- 3 G. Belford, R. L. Belford, J. F. Burkhaven, *J. Magn. Res.*, 1973, **11**, 2749.
- 4 Yu. V. Rakitin, G. M. Larin, V. V. Minin. *Interpretation of EPR spectrum of coordination compounds*. Publisher Science, 1993, 399.
- 5 Ya. S. Lebedev, V. I. Muromtsev. *EPR and relaxation of stabilized radicals*, Publisher Chemistry, 1972, 25.
- 6 M. J. Frisch, G. W. Trucks, H. B. Schlegel, G. E. Scuseria, M. A. Robb, J. R. Cheeseman, G. Scalmani, V. Barone, G. A. Petersson, H. Nakatsuji, X. Li, M. Caricato, A. V. Marenich, J. Bloino, B. G. Janesko, R. Gomperts, B. Mennucci, H. P. Hratchian, J. V. Ortiz, A. F. Izmaylov, J. L. Sonnenberg, D. Williams-Young, F. Ding, F. Lipparini, F. Egidi, J. Goings, B. Peng, A. Petrone, T. Henderson, D. Ranasinghe, V. G. Zakrzewski, J. Gao, N. Rega, G. Zheng, W. Liang, M. Hada, M. Ehara, K. Toyota, R. Fukuda, J. Hasegawa, M. Ishida, T. Nakajima, Y. Honda, O. Kitao, H. Nakai, T. Vreven, K. Throssell, J. A. Montgomery, Jr., J. E. Peralta, F. Ogliaro, M. J. Bearpark, J. J. Heyd, E. N. Brothers, K. N. Kudin, V. N. Staroverov, T. A. Keith, R. Kobayashi, J. Normand, K. Raghavachari, A. P. Rendell, J. C. Burant, S. S. Iyengar, J. Tomasi, M. Cossi, J. M. Millam, M. Klene, C. Adamo, R. Cammi, J. W. Ochterski, R. L. Martin, K. Morokuma, O. Farkas, J. B. Foresman, D. J. Fox, *GAUSSIAN 16 (Revision A.03)*, Gaussian, Inc., Wallingford, CT, 2016.
- 7 W. Kohn, L. J. Sham, *Physical Review*, 1965, **140**, A1133.
- 8 S. A. Nikolaevskii, M. A. Kiskin, A. A. Starikova, N. N. Efimov, A. A. Sidorov, V. M. Novotortsev, I. L. Eremenko, *Russ. Chem. Bull.*, 2016, **65**, 2812.
- 9 S. A. Nikolaevskii, I. S. Evstifeev, M. A. Kiskin, A. A. Starikova, A. S. Goloveshkin, V. V. Novikov, N.V. Gogoleva, A. A. Sidorov, I. L. Eremenko, *Polyhedron*, 2018, **152**, 61.
- 10 S. A. Nikolaevskii, M. A. Kiskin, A. G. Starikov, N. N. Efimov, A. S. Bogomyakov, V. V. Minin, E. A. Ugolkova, O. M. Nikitin, T. V. Magdesieva, A. A. Sidorov, I. L. Eremenko, *Russ. J. Coord. Chem.*, 2019, **45**, 273.
- 11 L. Noddleman, *J. Chem. Phys.*, 1981, **74**, 5737.
- 12 Y. Kitagawa, T. Saito, Y. Nakanishi, Y. Kataoka, T. Matsui, T. Kawakami, M. Okumura, K. Yamaguchi, *J. Phys. Chem. A*, 2009, **113**, 15041.
- 13 B. O. Roos, P. R. Taylor, P. E. M. Siegbahn, *Chem. Phys.*, 1980, **48**, 157.
- 14 S. Per, H. Anders, R. Björn, L. Bernard, *Phys. Scr.*, 1980, **21**, 323.
- 15 P. E. M. Siegbahn, J. Almlöf, A. Heiberg, B. O. Roos, *J. Chem. Phys.*, 1981, **74**, 2384.
- 16 C. Angeli, R. Cimiraglia, S. Evangelisti, T. Leininger, J. P. Malrieu, *J. Chem. Phys.*, 2001, **114**, 10252.
- 17 C. Angeli, R. Cimiraglia, J.-P. Malrieu, *Chem. Phys. Lett.*, 2001, **350**, 297.
- 18 C. Angeli, R. Cimiraglia, *Theor. Chem. Acc.*, 2002, **107**, 313.
- 19 C. Angeli, R. Cimiraglia, J.-P. Malrieu, *J. Chem. Phys.*, 2002, **117**, 9138.
- 20 B. A. Hess, *Phys. Rev. A*, 1986, **33**, 3742.
- 21 D. A. Pantazis, X. Y. Chen, C. R. Landis, F. Neese, *J. Chem. Theory Comput.*, 2008, **4**, 908.

- 22 A. Schafer, C. Huber, R. Ahlrichs, *J. Chem. Phys.*, 1994, **100**, 5829.
- 23 A. Schafer, H. Horn, R. Ahlrichs, *J. Chem. Phys.*, 1992, **97**, 2571.
- 24 F. Weigend, R. Ahlrichs, *Phys. Chem. Chem. Phys.*, 2005, **7**, 3297.
- 25 F. Neese, *J. Comput. Chem.*, 2003, **24**, 1740.
- 26 D. Ganyushin, F. Neese, *J. Chem. Phys.*, 2006, **125**, 024103.